The effect of pyridyl anchoring groups at the surfaces of Ru(II)-dye-sensitized TiO_2 nanoparticles on photocatalytic oxygen evolution

Hiroki Otsuka, Atsushi Kobayashi, Masaki Yoshida, and Masako Kato**

Department of Chemistry, Faculty of Science, Hokkaido University, North-10 West-8, Kita-ku, Sapporo 060-0810, Japan

Corresponding authors

Email: akoba@sci.hokudai.ac.jp (A.K.); mkato@sci.hokudai.ac.jp (M.K.).

Abstract

Photocatalytic oxygen evolution driven by two pyridyl-anchor-modified Ru(II) photosensitizers, namely $[Ru(bpy)_2(qpy)](PF_6)_2$ and $[Ru(qpy)_3](PF_6)_2$ (**RuPy^2** and **RuPy^6**; bpy = 2,2'-bipyridine, qpy = 2,2'-4,4''-4',4'''-quaterpyridine), was examined in order to investigate the influence of pyridyl groups as the connectors that bind both the water-oxidation and water-reduction catalysts. **RuPy^2** and **RuPy^6** act as redox photosensitizers in the presence of the $S_2O_8^{2-}$ sacrificial electron acceptor and the $K_{2x}Co_{(3-x)}[Fe(CN)_6]_2 \cdot nH_2O$, Prussian-blue-type, water-oxidation catalyst; however, their photosensitizing efficiencies were lower than that of $[Ru(bpy)_3]^{2+}$ because of their lower reactivities with $S_2O_8^{2-}$, probably due to steric hindrance associated with the pyridyl groups. Interestingly, the photosensitizing efficiency of **RuPy^2** was significantly improved through immobilization on TiO_2 nanoparticles (**RuPy^2@TiO$_2$**), while the efficiency of **RuPy^6** was hardly improved by immobilization. These contrasting results indicate that the surface structure of the photosensitizer-immobilized nanoparticle is a crucial factor that determines photosensitizing and/or photocatalytic activity.

Keywords

Photocatalyst, Water oxidation, Dye-sensitization, Artificial photosynthesis, Ru(II) complex

1. Introduction

As a promising approach that addresses the global energy issue, the solar water-splitting reaction has attracted considerable attention because it enables the conversion of the energy of sunlight into the chemical energy of dihydrogen (H_2) [1,2]. Since the pioneering work on TiO_2 by Honda and Fujishima [3], extensive effort has been devoted over several decades to the development of a variety of solar water-splitting systems, including those based on heterogeneous photocatalysts that use semiconductor materials [4-7], and homogeneous photocatalytic systems based on molecular materials [8-15]. Recently, photoelectrochemical (PEC) cells composed of semiconductor electrodes modified with photosensitizer (PS) dye molecules and/or molecular water-reduction/water-oxidation catalysts (WRCs/WOCs) have been extensively developed [16-17]. The interfaces between the PS dye (or semiconductor electrode) and the WRC and WOC in a PEC cell are critical factors that determine the light-driven water-splitting efficiency because the photoexcited electron must travel beyond these interfaces [18-22]. This is especially critical for the O_2-evolving photoanode because four electrons are transferred during the oxidation of a water molecule ($H_2O \rightarrow O_2 + 4H^+ + 4e^-$). One promising approach toward effective photoinduced-charge separation, which is referred to as the “through particle mechanism”, involves the use of semiconductor nanoparticles as the electron-transfer mediator. Reisner and co-workers reported that the combination of [NiFeSe]-hydrogenase and $[Ru(bpy)_3]^{2+}$-sensitized TiO_2 nanoparticles (bpy = 2,2′-bipyridine) enabled the production of H_2 even under aerobic conditions [23]. We recently reported on the multi-layered PS-dye structure of Pt-cocatalyst-loaded TiO_2 nanoparticles that act as an effective photoinduced-charge separating layer, such that photoexcited electron-hole pairs are separated to the insides and outer-edges of the nanoparticles [24]. However, the development of a highly effective photoinduced-

charge-separation WOC/WRC interface that facilitates the overall water-splitting reaction remains a challenge.

Our recent attention has focused on the interface between the PS dye and the WOC. Several recent progresses toward supramolecular photocatalysts for water oxidation suggest that photocatalytic O_2-evolution activity is improved by the coordination-bond assembly of a molecular PS and a WOC [25]. However, whether or not direct-bonding interactions between the PS and WOC are necessary to achieve high charge-separation efficiency remains unclear. Therefore, in order to investigate the effect of direct coordination bonding between the PS and the WOC, we selected two Ru(II)-polypyridine complexes, namely $[Ru(bpy)_2(qpy)]^{2+}$ and $[Ru(qpy)_3]^{2+}$ (**RuPy^2** and **RuPy^6**; see Scheme 1, qpy = 2,2'-4,4''-4',4'''-quaterpyridine), with two and six neutral pyridyl anchoring groups, respectively, as PS molecules for water oxidation in this work. Although **RuPy^6** has been reported by Hanan *et al.* to be a highly efficient PS for H_2 production [26,27], to the best of our knowledge, there is no report on the photocatalytic water-oxidation reaction driven by these pyridyl-functionalized $[Ru(bpy)_3]^{2+}$ analogues. In addition, we were also interested in the effect of **RuPy^n** (n= 2, 6) immobilization on the surfaces of TiO_2 nanoparticles on the photocatalytic O_2-evolution reaction because several pyridyl-anchor-modified dyes have been reported [28-30]; in particular Sakai and Ozawa firstly demonstrated that that a $[Ru(bpy)_3]^{2+}$-type photosensitizer can be more stably immobilized on the surface of TiO_2 using the pyridyl anchoring group compared to the widely used phosphonate-anchoring group [29-30]. The $K_{2x}Co_{(3-x)}[Fe(CN)_6]_2 \cdot nH_2O$ Prussian-blue analogue (hereafter CoFe-PBA) [31] was selected as the WOC, because the labile Co(II) sites on the surface of CoFe-PBA are expected to easily form coordination bonds with the pyridyl anchors of **RuPy^n**. In this report, we demonstrate that the pyridyl groups of the **RuPy^n** photosensitizers suppress reactivity with the

$Na_2S_2O_8$ sacrificial electron acceptor, but this detrimental effect is overcome by the immobilization of **RuPy^2** on the surfaces of TiO_2 nanoparticles.

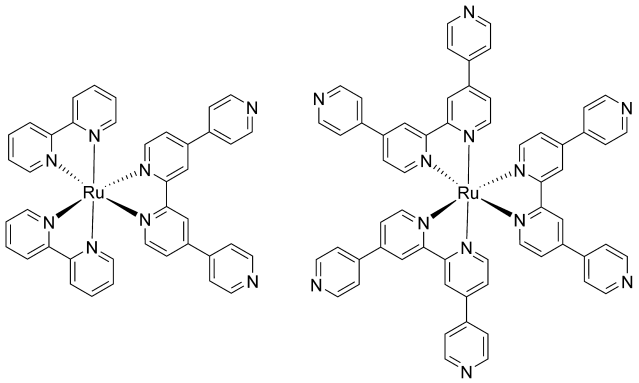

RuPy^2 $[Ru(bpy)_2(qpy)]^{2+}$ **RuPy^6** $[Ru(qpy)_3]^{2+}$

Scheme 1. The molecular structures of the Ru(II) photosensitizers used in this study.

2. Materials and Methods

2.1 Synthesis and Materials

2,2'-4,4''-4',4'''-Quaterpyridine (qpy) [32], $[Ru(bpy)_2(qpy)](PF_6)_2$ (**RuPy^2**) [26], $[Ru(bpy)_2(qpy)](PF_6)_2$ (**RuPy^6**) [27], and $[Ru(bpy)_3](SO_4)$ [33] were synthesized as previously reported. TiO_2 nanoparticles (SSP-M, ~ϕ15 nm) were purchased from the Sakai Chemical Industry Co. Ltd. The CoFe-PBA water-oxidation catalyst, was synthesized by a previously reported method [31].

2.1.1 Preparation of RuPy^n-immobilized TiO_2 nanoparticles (RuPy^n@TiO_2)

The TiO_2-nanoparticle powder (120.4 mg) was dispersed in a solution of **RuPy^n** (1.25 mM, 24 mL) in acetonitrile/toluene (2:3 v/v for **RuPy^2**, and 11:9 v/v for **RuPy^6**). The solution was stirred in the dark, overnight, at room temperature. The **RuPy^n**-immobilized TiO_2 nanoparticles obtained in this manner were isolated by ultracentrifugation (50000 rpm, 15 min), and the supernatant was removed. After washing twice with the reaction solvent, the isolated **RuPy^n@TiO$_2$** was dried under vacuo. The amount of immobilized **RuPy^n** on the TiO_2 nanoparticles was determined by UV-vis absorption spectroscopy of the supernatant (See Supporting Information, SI).

2.2 Measurements

UV−vis absorption spectra were recorded on a Shimadzu UV-2400PC spectrophotometer. Luminescence spectra were recorded on a JASCO FP-6600 spectrofluorometer at 298 K. Emission quantum yields (Φ_{em}) were measured using a Hamamatsu C9920-02 absolute photoluminescence quantum-yield-measurement system equipped with an integrating sphere apparatus and a 150-W continuous-wave xenon light source. Emission lifetime (τ) measurements were conducted using a Hamamatsu Photonics C4334 system equipped with a streak camera as the photodetector and a nitrogen laser as the excitation light source (λ_{ex} = 470 nm for **RuPy^2** and 474 nm for **RuPy^6**). Each sample solution was deoxygenated by bubbling with N_2 for 30 min at 298 K. Cyclic voltammetry (CV) was conducted using a Hokuto Denko HZ-3000 electrochemical measurement system equipped with glassy carbon, Pt wire, and Ag/Ag^+ electrodes as the working, counter, and reference electrodes, respectively. Ferrocene was used the internal standard. An acetonitrile solution containing 0.1 M tetrabutylammonium hexafluorophosphate ($TBAPF_6$), as the supporting electrolyte, and 1.0 mM of the Ru(II) complex, was used in the CV experiments. **RuPy^n**-immobilized TiO_2-modified FTO electrode

were prepared by literature method.[34] All solutions were deaerated by bubbling N_2 for 15 min prior to any measurement. IR spectra were recorded on a Jasco FT-IR 4100 spectrophotometer with KBr pellets. Zeta potential measurement and dynamic light scattering (DLS) analysis were conducted using an OTSUKA ELSZ-1000SCl analyzer.

2.3 Photochemical O_2-evolution Reaction

A phosphate-buffer-water/acetonitrile (2:1 v/v) solution (18 mM, pH 7.2) containing the Ru(II) photosensitizer (100 μM of the Ru(II) complex) and the water-oxidation catalyst (1 mg CoFe−PBA) was placed, in the dark, in a Pyrex vial (~15 mL volume) with a small magnetic stirring bar and covered with a rubber septum. A $Na_2S_2O_8$ solution (5, 10 mM) was injected into this mixed solution or dispersion by a syringe and the resultant solution (total 5 mL) was deoxygenated by bubbling with Ar gas for 30 min. A robust O_2 sensor probe (Pyro Science, FireSting O2 oxygen meter) was fitted to the top of the septum to detect the oxygen concentration within the headspace of the vial. The vial was irradiated with a blue LED lamp (λ = 470 ± 10 nm; 210 mW; OptoDevice Lab. Ltd., OP6-4710HP2) from underneath. The temperature was set to 293 K with a homemade aluminum water-cooling jacket and a temperature circulator (EYELA CCA-1111). Turnover numbers (TONs) and turnover frequencies (TOFs) were determined from the amount of evolved O_2; four photoredox cycles of the Ru(II) photosensitizer are required to oxidize one water molecule. The apparent quantum yield (Φ_{Ox}) was calculated using the following equation:

$$\Phi_{Ox} = N_e/N_p = 4N_{O_2}/N_p \quad (1),$$

where, N_e is the number of reacted electrons, N_{O_2} is the number of evolved O_2 molecules, and N_p is the number of incident photons.

3. Results and Discussion

3.1 Synthesis and Characterization

As mentioned in Introduction, the pyridyl group has been reported to be a useful organic anchor for immobilizing various functional molecules on TiO_2 electrodes. In order to investigate the differences in the immobilization behavior of **RuPy^2** and **RuPy^6**, we first measured the UV-vis absorption spectra of the supernatant solutions obtained following their immobilization reactions (Figure S1 and Table S1 in the SI). The amounts of immobilized **RuPy^n** on the TiO_2 nanoparticles are summarized in Table 1 and are compared with that of the previously reported **RuCP^2** phosphonate-functionalized Ru(II) photosensitizer [24]. The amounts of immobilized **RuPy^2** and **RuPy^6** are comparable with that of **RuCP^2**, indicating that the pyridyl groups of **RuPy^n** (n = 2, 6) act as effective anchors. It is interesting to note that the amount of immobilized **RuPy^6** was moderately higher than that of **RuPy^2** in spite of its bulkier molecular structure [27, 35]. The slightly larger amount of immobilized **RuPy^6** over **RuPy^2** implies that uncoordinated pyridyl groups contribute to arranging the molecular orientations of the immobilized molecules so as to form a more tightly packed structure on the surface. As shown in Figure 1, characteristic ^{1}MLCT absorptions were clearly observed at around 470 nm in the UV-vis diffuse reflectance spectra of the **RuPy^n**-immobilized TiO_2 nanoparticles (**RuPy^n**@TiO_2), indicating that the **RuPy^n** photosensitizing molecules were successfully immobilized on the TiO_2 surface. The slightly larger absorption band observed for **RuPy^6**@TiO_2 compared to **RuPy^2**@TiO_2 is ascribable to the larger molar absorption coefficient of the ^{1}MLCT band of **RuPy^6** than that of **RuPy^2**. The immobilization of positively-charged **RuPy^n** at the surface of TiO_2 nanoparticle was

also confirmed by the zeta potential measurements (Table S2); both **RuPy^2@TiO$_2$** and **RuPy^6**@TiO_2 exhibited positive zeta potential ranging from 11 to 28 mV, whereas the potential of non-modified TiO_2 nanoparticle was negative (-27 mV) because of the OH^- anions were thought to be coordinated to Ti(IV) ion at the TiO_2 surface.[36] The larger positive zeta potential of **RuPy^6**@TiO_2 than **RuPy^2**@TiO_2 is probably because the ratio of pyridyl-coordinated Ti(IV) site to uncoordinated (or OH-coordinated) Ti(IV) site is larger for **RuPy^6**@TiO_2 than **RuPy^2**@TiO_2 even in the comparable amount of the immobilized **RuPy^n** dye on the TiO_2 surface.

It is well known that the ^{3}MLCT emission of the $[Ru(bpy)_3]^{2+}$ molecular photosensitizer is strongly quenched by immobilization on TiO_2 [37]. In contrast, the each **RuPy^n** clearly exhibited a ^{3}MLCT emission band from the corresponding **RuPy^n@TiO$_2$** nanoparticles (Figure S2), although the intensities of the emissions from **RuPy^n@TiO$_2$** were weaker than those of their non-immobilized solution states, which is ascribable to excitation light scattering of the TiO_2 nanoparticles. Indeed, the emission quantum yield of **RuPy^2@TiO$_2$** was determined to be comparable (Φ = 0.07) to that observed in the solution state and the particle diameters of **RuPy^n@TiO$_2$** estimated by the dynamic light scattering method were distributed from sub-micron to several tens micron range (see Figure S3). This large difference in emission-quenching behavior between the well-known $[Ru(bpy)_3]^{2+}$ and **RuPy^n** probably originates from the longer emission wavelengths of **RuPy^n**. As shown in Figure S4, the ^{3}MLCT emission wavelengths of **RuPy^2** and **RuPy^6** at both 298 and 78 K are red-shifted (above 30 nm) with respect to the emission of $[Ru(bpy)_3]^{2+}$. Cyclic voltammetry experiments using the **RuPy^n** immobilized TiO_2/FTO working electrode clearly indicate that the Ru(III)/Ru(II) redox potential were negligibly affected by the immobilization to the TiO_2 surface probably due to the localization of

the HOMO at the central Ru(II) ion (Figure S5). As a result, the excited electron in the ^{3}MLCT state of **RuPy^n** does not have sufficient negative potential (Table S3) to be injected to the TiO_2

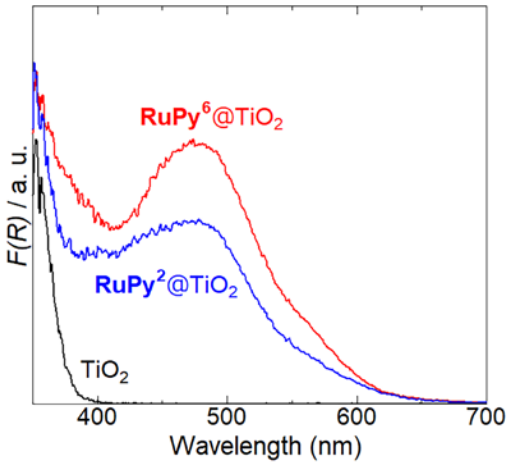

Figure 1. UV-vis diffuse reflectance spectra of **RuPy^n@TiO$_2$** (n = 2, 6) in the solid state at room temperature.

Table 1. Amounts of immobilized Ru(II) complexes on TiO_2 nanoparticle surfaces.

Complex	Amount of immobilized Ru(II) complex (nmol/mg TiO_2)	Surface coverage (nmol/cm^2)
RuPy^2	99.6	0.0971
RuPy^6	113	0.110
RuCP^2 [a]	116	0.113

[a] Ref. [24].

3.2 Photochemical O_2-evolution Reactions

Although several groups have reported photocatalytic hydrogen-evolution reactions driven by pyridyl-functionalized Ru(II) photosensitizers, such as **RuPy^{6}**, photocatalytic O_2-evolution catalyzed by such a pyridyl-functionalized Ru(II) PS has not been reported. We performed photocatalytic O_2-evolution experiments in the presence of molecular **RuPy^{n}** or the TiO_2-immobilized photosensitizers, with $Na_2S_2O_8$ as the sacrificial electron acceptor, the results of which are displayed in Figure 2, while TONs, TOFs, and Φ_{Ox} values are summarized in Table 2. Oxygen evolution was observed upon irradiation of each **RuPy^{n}**-containing sample with light, and the TONs of these reactions after 60 min of irradiation were above unity. Hence, O_2 was evolved through photocatalytic processes involving the **RuPy^{n}** photosensitizers. However, as shown in Figure 2(a), the TONs and TOFs of **RuPy^{2}** and **RuPy^{6}** were less than half and a quarter of those of $[Ru(bpy)_3]^{2+}$, respectively, in the presence of 5 mM $Na_2S_2O_8$ sacrificial electron acceptor. In contrast, it is noteworthy that both the TON and TOF of **RuPy^{2}** increased remarkably when immobilized on the surfaces of TiO_2 nanoparticles (**RuPy^{2}@TiO$_2$**), whereas such the improvement by immobilization was hardly observed for **RuPy^{6}@TiO$_2$**. Considering that both pyridyl groups of **RuPy^{2}** are coordinated to Ti^{4+} ions on the surfaces of the TiO_2 nanoparticles, the uncoordinated pyridyl groups of **RuPy^{n}** may suppress photoinduced charge separation between the photosensitizer, the sacrificial electron acceptor, and the water-oxidation catalyst. The photosensitizing efficiency of **RuPy^{n}** dyes in homogeneous system was improved by increasing the concentration (10 mM) of $Na_2S_2O_8$ sacrificial electron acceptor, indicating that the oxidative quenching of the photoexcited [**RuPy^{n}**]* by $S_2O_8^{2-}$ anion could be the rate determining step of photocatalytic O_2 evolution reaction. In contrast, completely different behaviors were observed for the heterogeneous systems, **RuPy^{2}**@TiO_2 and **RuPy^{6}**@TiO_2 (see Figures 2(b) and 2(c)); the efficiency of **RuPy^{2}**@TiO_2 strongly depended on the $S_2O_8^{2-}$

concentration whereas **RuPy^6**@TiO_2 exhibited negligible dependence on the $S_2O_8^{2-}$ concentration. These remarkably different behaviors between **RuPy^2**@TiO_2 and **RuPy^6**@TiO_2 indicate that the surface condition of the **RuPy^n** immobilized TiO_2 nanoparticle greatly influenced on the photocatalytic O_2 evolution activity.

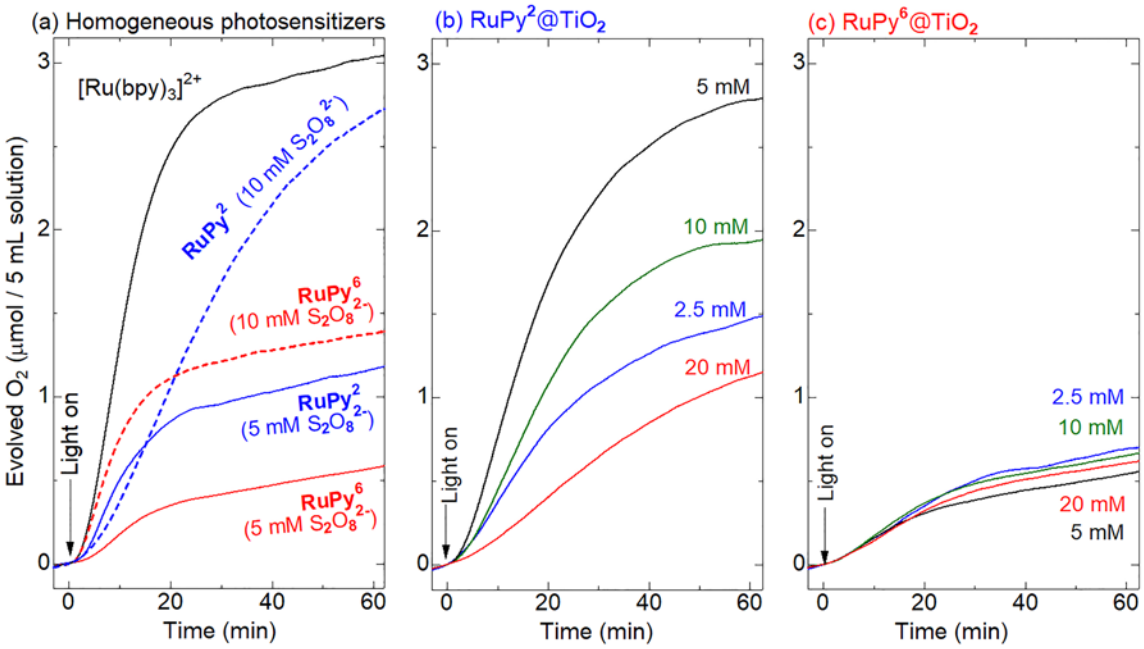

Figure 2. Photocatalytic O_2-evolution reactions driven by (a) homogeneous photosensitizer $[Ru(bpy)_3]^{2+}$ (black), **RuPy^2** (blue) and **RuPy^6** (red) or (b) heterogeneous photosensitizer **RuPy^2@TiO$_2$** and (c) **RuPy^6@TiO$_2$** (red) (100 μM of the Ru(II) complex) with CoFe-PBA (1 mg) in $Na_2S_2O_8$ sacrificial electron acceptor (2.5 to 20 mM) and 18 mM phosphate-buffer-water/acetonitrile (2:1 v/v) solution (pH 7.2) under an atmosphere of Ar. A blue LED (λ = 470 ± 10 nm) was used as the light source.

Table 2. Photocatalytic O_2-evolution-reaction results.

Photosensitizer	$Na_2S_2O_8$ concentration	O_2 (μmol) [a]	TON [a]	TOF (min^{-1}) [b]	Φ_{Ox} (%) [a]
$[Ru(bpy)_3]^{2+}$	5mM	3.03	24.3	1.04	0.409
RuPy^2	5 mM	1.17	9.32	0.400	0.157
	10 mM	2.69	21.6	0.339	0.362
RuPy^6	5 mM	0.572	4.57	0.141	0.0771
	10 mM	1.38	11.1	0.597	0.186
RuPy^2@TiO$_2$	2.5 mM	1.47	11.8	0.299	0.198
	5 mM	2.78	22.3	0.611	0.375
	10 mM	1.59	12.7	0.249	0.214
	20 mM	1.13	9.02	0.128	0.152
RuPy^6@TiO$_2$	2.5 mM	0.693	5.54	0.126	0.0933
	5 mM	0.541	4.32	0.127	0.0729
	10 mM	0.651	5.20	0.136	0.0877
	20 mM	0.606	4.85	0.113	0.0817

[a] After irradiation for 60 min. [b] After irradiation for 10 min.

To clarify the origin of the differences in the photosensitizing efficiencies of the three molecular photosensitizers, we performed emission-quenching experiments using $Na_2S_2O_8$ as a sacrificial electron acceptor. Stern-Volmer plots of **RuPy^6**, **RuPy^2**, and $[Ru(bpy)_3]^{2+}$ in the presence of various concentrations of $Na_2S_2O_8$ are shown in Figure 3. The calculated Stern-Volmer constant (K_{sv}), emission lifetime (τ_{em}), and quenching rate constant (k_q) of each complex are listed in Table 3. The quenching efficiencies of **RuPy^6**, and **RuPy^2** by $S_2O_8^{2-}$ were significantly lower than that of $[Ru(bpy)_3]^{2+}$ over the entire concentration range. The k_q value decreased in the order: $[Ru(bpy)_3]^{2+}$ >> **RuPy^2** > **RuPy^6**, suggesting that greater numbers of pyridyl-anchor-modified bpy ligands result in less-efficient quenching of the Ru(II) complex by

$S_2O_8^{2-}$. Considering that $[Ru(bpy)_3]^{2+}$ has previously been reported to form an ion-pair intermediate with $S_2O_8^{2-}$ during electron-transfer [39,40], the lower quenching efficiencies of **RuPy^n** (n = 2, 6) compared to that of $[Ru(bpy)_3]^{2+}$ are ascribable to suppression of ion-pair formation by the sterically bulky pyridyl groups of the qpy ligand(s). In contrast, comparable emission quenching (I^0/I ~ 1.5) using CoFe-PBA was observed for all three molecular photosensitizers (Figure S6), whereas the adsorption of these **RuPy^n** dyes to the surface of CoFe-PBA were confirmed by UV-Vis absorption spectral changes (Figure S7 and Table S4). These results suggest that the pyridyl groups of **RuPy^n** hardly affect their reactivities with the CoFe-PBA catalyst at the photoexcited state. Hence, the lower photosensitizing efficiencies of the **RuPy^n** (n = 2, 6) molecular photosensitizers toward the water-oxidation reaction compared to $[Ru(bpy)_3]^{2+}$ are due to the poorer reactivity of the sacrificial electron-accepting $S_2O_8^{2-}$ ion when sterically-bulky pyridyl groups are present.

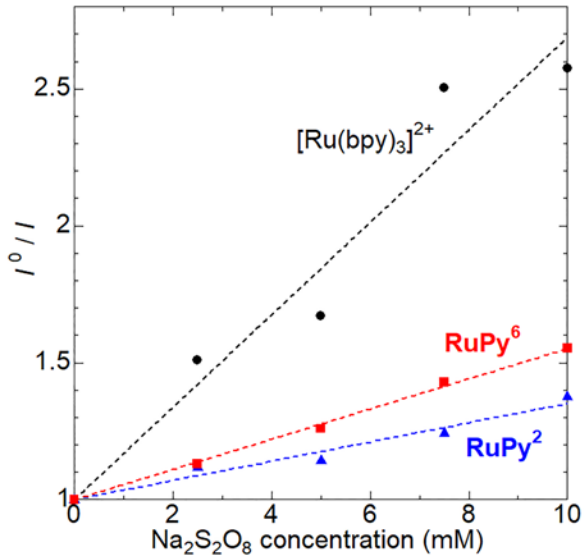

Figure 3. Stern–Volmer plots of 100 μM solutions of $[Ru(bpy)_3]^{2+}$ (black closed circles), **RuPy^2** (blue closed triangles), and **RuPy^6** (red closed triangles) in the presence of various

concentrations of $Na_2S_2O_8$ at room temperature. A 2:1 (v/v) mixture of H_2O/CH_3CN was used as the solvent during these experiments.

Table 3. Stern-Volmer and quenching rate constants for $[Ru(bpy)_3]^{2+}$, **RuPy^2**, and **RuPy^6**.

Photosensitizer	K_{sv} (mM^{-1}) [a]	k_q ($M^{-1}s^{-1}$) [b]
RuPy^6	0.0552	7.10×10^7
RuPy^2	0.0351	7.31×10^7
$[Ru(bpy)_3]^{2+}$	0.168	2.38×10^8

[a] Estimated from the slope of the Stern–Volmer plot displayed in Figure 3.
[b] Estimated using the equation: $k_q = K_{SV}/\tau_{em}$; the τ_{em} of each complex is listed in Table S3.

The immobilization of molecular photosensitizers onto the surfaces of TiO_2 nanoparticles generally tends to suppress their reaction efficiencies with sacrificial reagents and catalysts because of the slower diffusions of larger nanoparticles compared to those of single molecules. Nevertheless, the photosensitization efficiency of the immobilized **RuPy^2@TiO$_2$** was higher than that of its molecular equivalent, **RuPy^2** in the optimized condition (5 mM $Na_2S_2O_8$ solution). This result suggests that the immobilization of **RuPy^2** onto the TiO_2 nanoparticles provides benefits that compensate for slower nanoparticle diffusion, which is a plausible reason for the observed improvement in reactivity of the TiO_2-immobilized **RuPy^2** with the sacrificial $S_2O_8^{2-}$ acceptor. In contrast, such the enhancement by immobilization was hardly observed for **RuPy^6**. As discussed above, the uncoordinated pyridyl anchoring groups of the **RuPy^n** certainly suppress their reactivities with $S_2O_8^{2-}$, probably due to steric hindrance (Figure 3). In the case of **RuPy^2@TiO$_2$**, the bulky qpy ligands of the **RuPy^2** coordinate to the Ti^{4+} ions on the surfaces of the TiO_2 nanoparticles. Such a molecular arrangement of molecular **RuPy^2** on the surface may

negate the detrimental effects associated with the bulkiness of the uncoordinated pyridyl groups of the qpy ligand, resulting in higher photosensitization efficiency of the heterogeneous **RuPy^2@TiO$_2$** photosensitizer compared to that of homogeneous **RuPy^2**. Indeed, the **RuPy^2@TiO$_2$** emission was more effectively quenched by $S_2O_8^{2-}$ than that of **RuPy^2** (Figure S8). This assumption is also reasonable when considering the **RuPy^6**@TiO_2 results, that is, more than half of the pyridyl groups of **RuPy^6** remain uncoordinated in **RuPy^6**@TiO_2, and these groups face the outer edges of the **RuPy^6**@TiO_2 nanoparticles, resulting in low efficiency compared to that of **RuPy^6**. In addition, the positively charged surface of **RuPy^n**@TiO_2 nanoparticle may promote the electron transfer quenching process by the $S_2O_8^{2-}$ anionic sacrificial electron acceptor. In fact, the zeta potentials of both **RuPy^n**@TiO_2 was negatively shifted in the presence of $S_2O_8^{2-}$ (Table S2). Note that the contribution of photoinduced interfacial electron transfer from **RuPy^n*** to the TiO_2 nanoparticles would be negligible due to the lack of a Ru(III)/Ru(II)* redox potential (Scheme 2). Although the photosensitizing efficiency of **RuPy^2**@TiO_2 decreased by increasing $S_2O_8^{2-}$ concentration above 5 mM (Figure 2(b)), it would be due to the particle aggregation induced by the charge neutralization by surrounding $S_2O_8^{2-}$ anions around the positively-charged **RuPy^2**@TiO_2 nanoparticles as suggested by zeta potential shift (Table S2) and particle diameter changes estimated by dynamic light scattering (DLS) method (Figure S9). Such the aggregation of nanoparticles should suppress the reaction with both $S_2O_8^{2-}$ sacrificial acceptor and the CoFe-PBA catalyst because of the slower diffusion of aggregated nanoparticles. On the other hand, the photosensitizing efficiency of **RuPy^6**@TiO_2 hardly depended on the $S_2O_8^{2-}$ concentration. Although the reason is still under investigation, the pyridyl groups at the outer surface of **RuPy^6**@TiO_2 might bind the

CoFe-PBA catalyst, resulting in the lower efficiency of photo-induced electron transfer reaction from the surface-immobilized **RuPy^{6}*** to $S_2O_8^{2-}$ sacrificial acceptor.

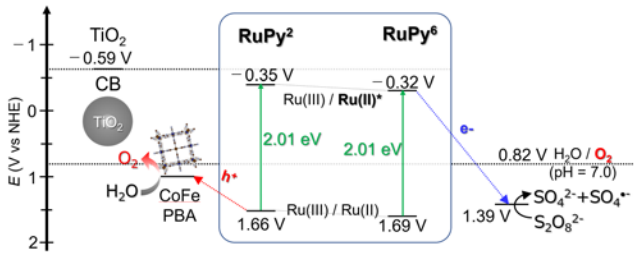

Scheme 2. Depicting a plausible electron-transfer mechanism for **RuPy^{n}@TiO$_2$** (n = 2, 6) during the photocatalytic O_2-evolution reaction. The redox potential of $S_2O_8^{2-}$ and the conduction-band minimum of TiO_2 are taken from the literature [38,41].

4. Conclusions

In this study, we immobilized pyridyl-anchor-functionalized Ru(II) photosensitizers (**RuPy^{n}**; n = 2, 6) on the surfaces of TiO_2 nanoparticles in order to investigate the effects of the pyridyl anchoring groups on the photocatalytic O_2-evolution reaction driven by the CoFe-PBA catalyst, which is a Prussian blue analogue. Emission-quenching experiments clearly indicate that the pyridyl groups of the **RuPy^{n}** molecular photosensitizers suppress their reactivities with the $S_2O_8^{2-}$ sacrificial electron acceptor, resulting in lower photocatalytic O_2-evolution activities in the presence of the CoFe-PBA catalyst than that of the unmodified $[Ru(bpy)_3]^{2+}$ complex. Although the ^{3}MLCT emission of the **RuPy^{n}** photosensitizers were hardly quenched by immobilization on the TiO_2 nanoparticles, the **RuPy^{2}**-loaded TiO_2 nanoparticles (**RuPy^{2}@TiO$_2$**) exhibited higher photocatalytic O_2-evolution activity under the same experimental condition than that of free **RuPy^{2}**, while the immobilization of **RuPy^{6}** on the TiO_2 nanoparticles hardly improved its activity. These contrasting results clearly indicate that the surfaces of the **RuPy^{n}**@TiO_2 nanoparticles have a dominating influence over the photocatalytic O_2-evolution reaction.

Acknowledgment

This study was supported by the Shimadzu Science Foundation, the Shorai Science and Technology Foundation, the Murata Science Foundation, Grants-in-Aid for Scientific Research (C)(26410063), Artificial Photosynthesis (area No. 2406, No.15H00858), and Soft Crystals (area No. 2903, No. JP17H06367) from MEXT, Japan.

References

[1] M.G. Walter, E.L. Warren, J.R. McKone, S.W. Boettcher, Q. Mi, E.A. Santori, N.S. Lewis, Solar water splitting cells, Chem. Rev. 110 (2010) 6446–6473.

[2] D.L. Ashford, M.K. Gish, A.K. Vannucci, M.K. Brennaman, J.L. Templeton, J.M. Papanikolas, T.J. Meyer, Molecular chromophore-catalyst assemblies for solar fuel applications, Chem. Rev. 115 (2015) 13006–13049.

[3] A. Fujishima, K. Honda, Electrochemical photolysis of water at a semiconductor electrode, Nature 238 (1972) 37–38.

[4] A. Kudo, Y. Miseki, Heterogeneous photocatalyst materials for water splitting, Chem. Soc. Rev. 38 (2009) 253–278.

[5] D.G. Nocera, The artificial leaf, Acc. Chem. Res. 45 (2012) 767–776

[6] Q. Wang, T. Hisatomi, Q. Jia, H. Tokudome, M. Zhong, C. Wang, Z. Pan, T. Takata, M. Nakabayashi, N. Shibata, Y. Li, I. D. Sharp, A. Kudo, T. Yamada, K. Domen, Scalable water splitting on particulate photocatalyst sheets with a solar-to-hydrogen energy conversion efficiency exceeding 1%, Nat. Mater. 15 (2016) 611–615.

[7] M. Zhu, Z. Sun, M. Fujitsuka, T. Majima, Z-scheme photocatalytic water splitting on a 2D heterostructure of black phosphorus/bismuth vanadate using visible light, Angew. Chem. Int. Ed. 57 (2018) 2160–2164.

[8] F.P. Rotzinger, S. Munavalli, P. Comte, J.K. Hurst, M. Graetzel, F.J. Pern, A.J. Frank, A molecular water-oxidation catalyst derived from ruthenium diaqua bis(2,2’-bipyridyl-5,5’-dicarboxylic acid), J. Am. Chem. Soc. 109 (1987) 6619–6626.

[9] L. Duan, F. Bozoglian, S. Mandal, B. Stewart, T. Privalov, A. Llobet, L. Sun, A molecular ruthenium catalyst with water oxidation activity comparable to that of photosystem II, Nat. Chem. 4 (2012) 418–423.

[10] M. Okamura, M. Kondo, R. Kuga, Y. Kurashige, T. Yanai, S. Hayami, V.K.K. Praneeth, M. Yoshida, K. Yoneda, S. Kawata, S. Masaoka, A pentanuclear iron catalyst designed for water oxidation, Nature 530 (2016) 465–468.

[11] H. Ozawa, M. Haga, K. Sakai, A photo-hydrogen-evolving molecular device driving visible-light-induced EDTA-reduction of water into molecular hydrogen. J. Am. Chem. Soc., 128 (2006) 4926-4927.

[12] M.S. Lowry, J. I. Goldsmith, J. D. Slinker, R. Rohl, R. A. Pascal, G.G. Malliaras, S. Bernhard, Single-layer electroluminescent devices and photoinduced hydrogen production from an ionic iridium(III) complex, Chem. Mater. 17 (2005) 5712–5719.

[13] M. L. Helm, M. P. Stewart, R. M. Bullock, M. R. DuBois, D. L. DuBois, A synthetic nickel electrocatalyst with a turnover frequency above 100,000 s^{-1} for H_2 production. Science 333 (2011) 863-866.

[14] R. S. Khnayzer, C. E. McCusker, B. S. Olaiya, F. N. Castellano, Robust cuprous phenanthroline sensitizer for solar hydrogen photocatalysis. J. Am. Chem. Soc. 135 (2013) 14068−14070.

[15] Y. Tsuji, K. Yamamoto, K. Yamauchi, K. Sakai, Near-infrared-light-driven hydrogen evolution from water using a polypyridyl triruthenium photosensitizer, Angew. Chem. Int. Ed. 57 (2018) 208-212.

[16] D.L. Ashford, M.K. Gish, A.K. Vannucci, M.K. Brennaman, J.L. Templeton, J.M. Papanikolas, T.J. Meyer, Molecular chromophore−catalyst assemblies for solar fuel applications, Chem. Rev. 115 (2015) 13006–13049.

[17] M. Yamamoto, L. Wang, F. Li, T. Fukushima, K. Tanaka, L. Sun, H. Imahori, Visible light-driven water oxidation using a covalently-linked molecular catalyst–sensitizer dyad assembled on a TiO_2 electrode. Chem. Sci. 7 (2016) 1430–1439.

[18] T. Kajiwara, K. Hashimoto, T. Kawai, T. Sakata, Dynamics of luminescence from $Ru(bpy)_3Cl_2$ adsorbed on semiconductor surfaces, J. Phys. Chem. 86 (1982) 4516–4522.

[19] W. Song, M.K. Brennaman, J.J. Concepcion, J.W. Jurss, P.G. Hoertz, H. Luo, C. Chen, K. Hanson, T.J. Meyer, Interfacial electron transfer dynamics for $[Ru(bpy)_2((4,4'\text{-}PO_3H_2)_2bpy)]^{2+}$ sensitized TiO_2 in a dye-sensitized photoelectrosynthesis cell: Factors influencing efficiency and dynamics, J. Phys. Chem. C 115 (2011) 7081–7091.

[20] P.G. Giokas, S.A. Miller, K. Hanson, M.R. Norris, C.R.K. Glasson, J.J. Concepcion, S.E. Bettis, T.J. Meyer, A.M. Moran, Spectroscopy and dynamics of phosphonate-derivatized ruthenium complexes on TiO_2, J. Phys. Chem. C 117 (2013) 812–824.

[21] W. Song, A. Ito, R.A. Binstead, K. Hanson, H. Luo, M.K. Brennaman, J.J. Concepcion, T.J. Meyer, Accumulation of multiple oxidative equivalents at a single site by cross-surface electron transfer on TiO_2, J. Am. Chem. Soc. 135 (2013) 11587–11594.

[22] D.F. Zigler, Z.A. Morseth, L. Wang, D.L. Ashford, M.K. Brennaman, E.M. Grumstrup, E.C. Brigham, M.K. Gish, R.J. Dillon, L. Alibabaei, G.J. Meyer, T.J. Meyer, J.M. Papanikolas,

Disentangling the physical processes responsible for the kinetic complexity in interfacial electron transfer of excited Ru(II) polypyridyl dyes on TiO_2, J. Am. Chem. Soc. 138 (2016) 4426–4438.

[23] E. Reisner, J.C. Fontecilla-Camps, F.A. Armstrong, Catalytic electrochemistry of a [NiFeSe]-hydrogenase on TiO_2 and demonstration of its suitability for visible-light driven H_2 production, Chem. Commun. 45 (2009) 550–552.

[24] S. Furugori, A. Kobayashi, A. Watanabe, M. Yoshida, M. Kato, Impact of photosensitizing multilayered structure on ruthenium(II)-dye-sensitized TiO_2-nanoparticle photocatalysts, ACS Omega 2 (2017) 3901–3912.

[25] L. Wang, M. Mirmohades, A. Brown, L. Duan, F. Li, Q. Daniel, R. Lomoth, L. Sun, L. Hammarström, Sensitizer-catalyst assemblies for water oxidation, Inorg. Chem. 54 (2015) 2742–2751.

[26] E. Rousset, D. Chartrand, I. Ciofini, V. Marvaud, G.S. Hanan, Facile one-pot synthesis of ruthenium(II) quaterpyridine-based photosensitizers for photocatalyzed hydrogen production, Inorg. Chem. 56 (2017) 9515–9524.

[27] E. Rousset, D. Chartrand, I. Ciofini, V. Marvaud, G.S. Hanan, Red-light-driven photocatalytic hydrogen evolution using a ruthenium quaterpyridine complex, Chem. Commun. 51 (2015) 9261–9264.

[28] L. Zhang, J.M. Cole, Anchoring groups for dye-sensitized solar cells, ACS Appl. Mater. Interfaces. 7 (2015) 3427–3455.

[29] K. Takijiri, K. Morita, T. Nakazono, K. Sakai, H. Ozawa, Highly stable chemisorption of dyes with pyridyl anchors over TiO_2: Application in dye-sensitized photoelectrochemical water reduction in aqueous media, Chem. Commun. 53 (2017) 3042–3045.

[30] K. Morita, K. Takijiri, K. Sakai, H. Ozawa, A platinum porphyrin modified TiO_2 electrode for photoelectrochemical hydrogen production from neutral water driven by the conduction band edge potential of TiO_2, Dalton Trans. 46 (2017) 15181–15185.

[31] S. Goberna-Ferrón, W.Y. Hernández, B. Rodríguez-García, J.R. Galán-Mascarós, Light-driven water oxidation with metal hexacyanometallate heterogeneous catalysts, ACS Catal. 4 (2014) 1637–1641.

[32] R.J. Morgan, A.D. Baker, 2,2':4,4":4',4"'-quaterpyridyl: a building block for the preparation of novel redox reagents. 1. Preparation and quaternization, J. Org. Chem. 55 (1990) 1986–1993.

[33] B.P. Sullivan, D.J. Salmon, T.J. Meyer, Mixed phosphine 2,2'-bipyridine complexes of ruthenium, Inorg. Chem. 17 (1978) 3334–3341.

[34] H. Ozawa, S. Honda, D. Katano, T. Sugiura, H. Arakawa, Novel ruthenium sensitizers with a dianionic tridentate ligand for dye-sensitized solar cells: the relationship between the solar cell performances and the electron-withdrawing ability of substituents on the ligand, Dalton Trans. 43 (2014) 8026-8036.

[35] P. Shi, B. J. Coe, S. Sánchez, D. Wang, Y. Tian, M. Nyk, and M. Samoc, Uniting ruthenium(II) and platinum(II) polypyridine centers in heteropolymetallic complexes giving strong two-photon absorption, Inorg. Chem. 54 (2015) 11450–11456.

[36] J. Zhao, H. Hidaka, A. Takamura, E. Pelizzetti, N. Serpone, Photodegradation of surfactants. 11. ζ-potential measurements in the photocatalytic oxidation of surfactants in aqueous TiO_2 dispersions, Langmuir 9 (1993) 1646–1650.

[37] W.D.K. Clark, N. Sutin, Spectral sensitization of n-type TiO_2 electrodes by polypyridineruthenium(II) complexes, J. Am. Chem. Soc. 99 (1977) 4676–4682.

[38] G. Rothenberger, D. Fitzmaurice, M. Grätzel, Spectroscopy of conduction band electrons in transparent metal oxide semiconductor films: Optical determination of the Fiat-band potential of colloidal titanium dioxide films, J. Phys. Chem. 96 (1992) 5983–5986.

[39] H.S. White, W.G. Becker, A.J. Bard, Photochemistry of the tris(2,2'-bipyridine) ruthenium(II)-peroxydisulfate system in aqueous and mixed acetonitrile-water solutions. Evidence for a long-lived photoexcited ion pair, J. Phys. Chem. 88 (1984) 1840–1846.

[40] Alexey L. Kaledin, Zhuangqun Huang, Yurii V. Geletii, Tianquan Lian, Craig L. Hill, Djamaladdin G. Musaev, Insights into photoinduced electron transfer between $[Ru(bpy)_3]^{2+}$ and $[S_2O_8]^{2-}$ in water: Computational and experimental studies, J. Phys. Chem. A 114 (2010) 73–80.

[41] U. Fürholz, A. Haim, Kinetics and mechanisms of the reactions of mononuclear and binuclear ruthenium(II) ammine complexes with peroxydisulfate, Inorg. Chem. 26 (1987) 3243–3248.